Appl. Comput. Harmon. Anal. 28 (2010) 285–295

Contents lists available at ScienceDirect

Applied and Computational Harmonic Analysis

www.elsevier.com/locate/acha

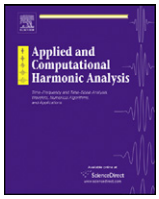

A wavelet cross-spectral analysis of solar–ENSO–rainfall connections in the Indian monsoons

Roddam Narasimha *, Subarna Bhattacharyya [1]

Engineering Mechanics Unit, Jawaharlal Nehru Centre for Advanced Scientific Research, Jakkur, Bangalore, India

ARTICLE INFO

Article history:
Received 7 July 2009
Revised 25 January 2010
Accepted 19 February 2010
Available online 26 February 2010
Communicated by Ginette Saracco

Keywords:
Wavelet analysis
Cross-spectra
El Nino-Southern Oscillation
Solar activity
Indian monsoon rainfall

ABSTRACT

The possible connections between the El Nino-Southern Oscillation (ENSO) phenomenon and Indian monsoon rainfall have been widely discussed in the meteorological literature. We show strong statistical evidence here for connections of ENSO with solar activity. This is particularly evident in a comparison between the two contrasting test periods of 1878–1913 and 1933–1964, representing three complete cycles of lowest and highest solar activity respectively since 1850. Wavelet statistical analysis reveals that the link between solar activity and ENSO is generally stronger than that between ENSO and rainfall but only slightly weaker than that between solar activity and rainfall. Over the two test periods an increase in solar activity is associated with a decrease in ENSO indices and an increase in the monsoon rainfall in the 8–16 y period band. In the 2–7 y period band the effects vary with region. The net effect of solar processes on rainfall thus appears to be the result of counteracting or cooperating influences on shorter (about 5–6 y) and longer (about 11–12 y) time scales, the latter on the whole dominating over the former. The present analysis thus suggests that the influence of solar processes on Indian rainfall operates in part indirectly through ENSO, but on more than one time scale.

1. Introduction

Association between solar processes and climate indices on long time scales of centuries to millennia [1,2,14,4,8,16,11,24,23] is now well established. The evidence for connections between solar activity and rainfall on shorter multi-decadal scales has also become stronger [27,34,9,3,4]. In this context, an important factor which is of much relevance to current climate change research is the El Nino-Southern Oscillation phenomenon (ENSO). Several studies ([31], [32] and the references therein, and [15]) on the impact of ENSO on Indian monsoon rainfall describe the temporal variability of the ENSO–monsoon interaction on the 2–7 y time scale. These and earlier studies suggest that ENSO and Indian monsoon share an inverse phase relationship, an ENSO-year being generally associated with below-normal monsoon rainfall. More recently, it has been found that Pacific SST (Sea Surface Temperature) anomaly *tendencies* (to be defined below) affect the All-India Summer Monsoon Rainfall (AISMR) to a larger extent than the SST anomalies themselves do [27]. (The anomalies in SST are usually measured over specific areas in the Pacific designated as Nino 3, Nino 3.4, etc.; their values over the months December, January and February are subtracted from those over the succeeding months March, April and May to get the SST anomaly *tendency* relevant to the rainfall of the monsoon season beginning in May–June.) A positive SST Nino 3.4 anomaly tendency, for example, represents a strong El Nino over the Pacific, which in turn results in weakening of the monsoon circulation over Asia, and vice versa.

* Corresponding author. Fax: +91 80 2208 2951.
E-mail addresses: roddam@caos.iisc.ernet.in (R. Narasimha), subarnabhattacharyya@yahoo.com (S. Bhattacharyya).
[1] Present address: Risk Management Solutions, Inc., 7015 Gateway Blvd, Newark, CA 94560, USA.

1063-5203/$ – see front matter
doi:10.1016/j.acha.2010.02.005

A study by Mehta and Lau [20] on multi-decadal variations reported that while solar irradiance and AISMR covary with nearly the same phase, Nino 3 SST covaries with solar irradiance with opposite phase. Their study also indicated the possibility that the multi-decadal irradiance component (accounting for 42% of the variance) influences the monsoon more than the 11 year component (30%) does.

All the processes and time series associated with monsoon rainfall, ENSO and solar activity are generally both non-stationary and nonlinear. The wavelet transform invented by Jean Morlet in the 80s therefore turns out to be a most appropriate tool for a study of the present kind. The known multi-decadal variability of the ENSO–monsoon system, together with the insight gained by the use of wavelet techniques [6,29,30] on the variability of the Indian monsoon [13,22] and its connection with solar activity [3,4], have led us to undertake the present study. Our main objective here is to present a wavelet-based analysis of the connections among the solar–ENSO–monsoon 'triad' using band-averaged wavelet power and cross power. Since we have earlier reported the results for solar–rainfall connections over Indian homogeneous-rainfall zones (as will be discussed in detail in Section 2 (ii)), it suffices here to focus on the evidence for the ENSO–solar connections in comparison to ENSO–rainfall and solar–rainfall connections.

A discussion of the mechanism that may be responsible for the effect of solar activity on ENSO is outside the scope of this paper. Nevertheless it is worth mentioning the analysis of Kodera [14], who finds that warming over the equatorial region is prominent during low solar activity, so the mechanism cannot be a simple absorption of solar energy by the oceans: the Sun does not directly exert an influence over sea-surface temperature. Instead, Kodera proposes that solar influence on the equatorial troposphere originates from the equatorial stratosphere through changes in the meridional circulation. This circulation modulates the *vertical extent* of convective activity as well as its horizontal distribution along the equator. In a paper published after the present script was submitted, Meehl et al. [21] propose that the above 'top–down' explanation is reinforced by the 'bottom–up' mechanism of a coupled oceans–atmosphere surface response. Neither Kodera nor Meehl et al. [21] focus on demonstrating a statistical relationship between solar activity and the ENSO cycle; Kodera further notes that the relation to the Indian monsoon needs to be studied. Our analysis is therefore complementary to Kodera's on both counts.

2. The present approach

The statistical significance of cross-spectra is often tested by a procedure devised by Torrence and Compo [30], to be briefly described in Section 5. This procedure has certain limitations when applied to the present problem, as pointed out by us earlier [4]. The first of these is connected with the very definition of the cross-spectrum (see Section 4), which is dominated by the strong periodic component in the sunspot time series (as we shall see below), even when the other signal in the pair is noise. The second is the statistical testing procedure, and the inappropriateness of the red noise reference spectrum P_k adopted when one of the signals has relatively long periods (e.g. sunspot number). Such limitations have been commented upon also by Maraun and Kurths [19].

However earlier work by the authors [3,4] was able to overcome these limitations and show much stronger statistical evidence for the effect of solar activity on monsoon rainfall than had previously been possible. The stronger evidence was the result of using the following new principles in assessing the effect of solar activity.

(i) For any parameter of interest (e.g. rainfall) we compare its average over each of two test periods (TP1, TP2 say, respectively 1878–1913 and 1933–1964) which exhibit the maximum contrast in solar activity over the time-span of available data. If the parameter is influenced by solar activity, we may then expect maximum contrast also in the values of the parameter over the same test periods. A comparison of averages over a sample size of order 30 (approximately the number of years in each test period) also enables us to carry out more meaningful statistical testing on the highly fluctuating signals we are investigating (see, e.g., Fig. 1). It turns out that the two periods can be selected in such a way that each comprises an integral number of solar cycles (3 in the present case). If a longer test period of 5 cycles is selected, the contrast in solar activity is necessarily lower; and, although the nature of the effect of solar activity (e.g. higher rainfall accompanies greater activity) remains qualitatively the same, the confidence level at which the difference can be asserted diminishes. The choice of such test periods also serves to ensure that the statistical non-stationarity, which characterizes ENSO, rainfall and solar activity on longer time scales (as is already evident from Fig. 1, see also [3]), is properly taken into account in the analysis. The centers of the two test periods are about 53 years apart from each other; the autocorrelation coefficient of the main rainfall index we use (called HIM; see (ii) below) fluctuates between $+/-$ 0.2 for lags of 2 or more years, such fluctuations presumably being chiefly statistical in character. For all these reasons the two test periods can be considered to be largely independent of each other.

(ii) India is meteorologically heterogeneous. It follows that the much used All-India Summer Monsoon Rainfall index, although useful in its own way, may well show a weaker effect of such variables as solar activity than do the regional rainfall-homogeneous zones, such as those proposed by Parthasarathy et al. [25,26]. The reason is that the homogeneous zones, each of which may be expected to be governed by similar dynamics, can carry a stronger signature, whereas averaging over heterogeneous zones can dilute the effect sought to be detected. This effect is real as we have shown [4] that there is noticeable regional differentiation in the effect of solar activity on rainfall.

(iii) Finally we use wavelet cross-spectra between different variables of interest as a primary statistics, and compare their values for rainfall-homogeneous zones over the test periods of (i). Furthermore, because of the peculiar problems as-

sociated with solar activity being one of the variables, namely the presence therein of a much stronger cycle than in any atmospheric variable, wavelet cross-spectra (e.g. between sunspot numbers and white noise, see [4]) can have misleadingly high values. We therefore use a special Monte Carlo method for statistical testing. In this method we first generate spectrally- or amplitude-matched synthetic noise and compare the cross-spectra of sunspot numbers with the atmospheric variable and with its matched noise respectively, and use the difference between them to assess the significance of the former. In analyzing cross-spectra we find it useful to consider appropriate band-averages. Because of the nonlinearities in the various processes involved, we cannot expect pure line frequencies in the variables of interest. For example, Friis-Christensen and Lassen [9] have shown that the solar cycle has a length varying from 9 to 13 y. Consideration of band averages therefore becomes necessary: it is not enough to track an 11.6 y period since it is no more than an average value.

Principles (i) to (iii) all enhance any signature of solar activity that might be present in the variable under study (rainfall or ENSO index), thus making it possible to compare data-segments that have experienced potentially the strongest effects of solar activity.

We demonstrate the application of these principles in the following analysis.

3. The data analyzed

The set of data analyzed in our work includes the time series for global SST ENSO index, Nino 3 and Nino 3.4 SST anomalies and tendencies, the sunspot numbers, solar irradiance, the all-India summer monsoon (AISM) rainfall, and the homogeneous rainfall data sets compiled by Parthasarathy et al. [25] over the period 1871–1990. The time step used in each of these time series is a year. The sunspot index data have been obtained from [28] and [7] (see also [24] for an early wavelet analysis). As the present analysis is chiefly demonstrative, we confine our attention almost entirely to rainfall in the homogeneous Indian monsoon (HIM) region, Nino 3.4 tendency and sunspot numbers. (The HIM region covers 55% of the land area of India towards the west and north-west, and is dominated by the south-west monsoon.) A more comprehensive treatment from a climatological perspective, covering other monsoon rainfall data sets and ENSO indices as well as solar irradiance, will be published separately.

The data for Nino region 3 SST anomalies in degrees Celsius are discussed and presented as figures in Trenberth [33]. The Nino 3.4 region is bounded by 120W–170W and 5S–5N. An ASCII text version of the file containing Nino 3.4 data may be obtained at ftp://ftp.cgd.ucar.edu/pub/CAS/TNIN34. The raw SST data is from the NOAA Climate Prediction Center at the website http://www.cpc.ncep.noaa.gov/data/. The tendencies relevant to the Indian monsoon season beginning in May–June have been computed for Nino 3.4 SST by subtracting the anomalies in SST over the preceding months December, January and February from those over March, April and May.

4. Wavelet notation

We use the continuous transform, with the Morlet wavelet function given by

$$\Psi_0(\eta) = \pi^{-1/4} e^{i\omega_0\eta} e^{-\eta^2/2}, \tag{1}$$

where ω_0 is a nondimensional frequency, taken equal to 6 in order to satisfy the wavelet admissibility condition [30], and η is a nondimensional time parameter. A discrete sequence R_n, $n = 0, \ldots, (N-1)$, possesses the continuous wavelet transform

$$W_n^R(s) = \sum_{n'=0}^{N-1} R_{n'} \Psi^* \left[\frac{(n'-n)\delta t}{s} \right], \tag{2}$$

where the star denotes the complex conjugate, and δt is the (sampling) time interval between two consecutive points in the time series. The wavelet function Ψ at each scale s is normalized to have unit energy. The wavelet power spectrum of R_n is given by the convolution $W_n^R(s)$, and the wavelet power by the magnitude $|W_n^R(s)[W_n^R(s)]^*|$. A time-average over all the local wavelet spectra gives the global wavelet spectrum,

$$\overline{\left(W^R\right)^2}(s) = \frac{1}{N} \sum_{n=0}^{N-1} \left| W_n^R(s) \right|^2. \tag{3}$$

The wavelet cross-spectrum $W_n^{RS}(s)$ between any two time series $R(t)$ and $S(t)$, with the respective wavelet transforms $W_n^R(s)$ and $W_n^S(s)$, is the complex quantity

$$W_n^{RS}(s) = W_n^R(s)\left[W_n^R(s)\right]^*, \tag{4}$$

whose absolute magnitude $|W_n^{RS}(s)|$ is the wavelet cross power. The global wavelet cross power is

$$\overline{W}^{RS}(s) = \frac{1}{N} \sum_{n=0}^{N-1} \left| W_n^{RS}(s) \right|. \tag{5}$$

The wavelet power averaged over a band b, given by s_j in steps of δj over $j_1 \leqslant j \leqslant j_2$, is the weighted sum $R_b^S(t)$ of the wavelet power spectrum over the band [30],

$$R_b^S(t) = \frac{\delta j \delta t}{C_\delta} \sum_{j_1}^{j_2} \frac{|W_n^S(s_j)|}{s_j}, \tag{6}$$

where $s_j = s_0 2^{j\delta j}$, $j = 0, 1, \ldots, J$, and $J = \delta j^{-1} \log_2(N\delta t/s_0)$. (Here $s_0 = 0.5$ y as we work on yearly data.) We choose $\delta j = 0.25$ y in order to obtain a reasonably fine resolution in scale. The constant $C_\delta = 0.776$ is the scale-independent reconstruction factor for the Morlet function [28].

Similarly the band-averaged wavelet cross power $R_b^{RS}(t)$ is a weighted sum of the wavelet cross power spectrum over the band b,

$$R_b^{RS}(t) = \frac{\delta j \delta t}{C_\delta} \sum_{j_1}^{j_2} \frac{|W_n^{RS}(s_j)|}{s_j}. \tag{7}$$

This may be the most appropriate place to point out that in the wavelet maps we present, we always mark the cone of influence within which the edges of our data stretch affect the wavelet transform. Results within the cone of influence must therefore be treated with caution. Similarly, because of the resolution of the data we use, the characteristics we analyze here are limited to wavelet scales longer than two years. However, as the present analysis is not concerned with shorter scales, this restriction is not relevant.

5. Significance testing

Three statistical significance testing schemes have been adopted here.

First is the standard z-test, used here to test whether differences between band-averaged coefficients in different test periods are significant; see the end of the section for a more specific description of the test and also [3,4]. The second is the Torrence–Compo test, in which a peak in the wavelet power spectrum is accepted at a certain percentage confidence level if it is significantly above a background or reference spectrum given by

$$P_k = \frac{1-\alpha}{1+\alpha^2 - 2\alpha\cos(2\pi k/N)}. \tag{8}$$

Here $k = 0, \ldots, N/2$ is the frequency index, and $\alpha = (\alpha_1 + \sqrt{\alpha_2})/2$ where α_1 and α_2 are the lag-1 and lag-2 autocorrelation coefficients of the time series under consideration. For a white noise background spectrum $\alpha = 0$, $P_k = 1$.

If the two time series $R_n(t)$ and $S_n(t)$ have background spectra given respectively by P_k^R and P_k^S, then according to [30] the cross wavelet power distribution is given by

$$\frac{|W_n^{RS}(s)|}{\sigma_R \sigma_S} \Rightarrow \frac{Z_\nu(p)}{\nu} \sqrt{P_k^R P_k^S}, \tag{9}$$

where σ_R and σ_S are the standard deviations of R and S respectively, ν is the number of degrees of freedom with which χ^2 is distributed, p denotes the level of confidence and $Z_\nu(p)$ denotes the value of the χ^2 distribution with ν degrees of freedom at the confidence level p. For the complex Morlet wavelet $\nu = 2$.

Now it has been shown [4] that the Torrence–Compo procedure suggests unduly high significance levels for a cross-spectrum when one of the time-series (solar activity in the present case) has a strong long-period oscillation. This can be easily demonstrated by analyzing the cross-spectrum of solar activity with white noise. We therefore also use a third testing scheme, which is a new Monte Carlo type procedure [4]. In this procedure the cross-spectrum under question is compared against that between solar activity and a specially generated synthetic noise time series. The synthetic noise may match the frequency spectrum (SN, for 'spectrally matched' noise) or the amplitude probability distribution (AN, for 'amplitude matched' noise) of the time series being analyzed, or even both [18] and will be called signal-matched (rainfall- or ENSO-matched, as may be the case). As spectrally matched noise is more stringent than amplitude-matched noise, we present results only for the former.

The statistical significance of the difference in solar-signal and solar-noise cross-spectra is then assessed using standard statistical tests. The results for solar–rainfall connections over all-India homogeneous rainfall zones have already been presented [4], so it suffices to show here the ENSO–solar connections in comparison to ENSO–rainfall connections.

The spectrally matched synthetic noise signals are generated using the spectral representation method of Grigoriu [10]. All cross-spectra with signal-matched noise are computed over an ensemble of 1000 realizations of 120 samples each. This ensemble size was found to be large enough to yield robust estimates for the cross-spectra, by comparing with results from a larger ensemble of 4000 realizations. This assures us that we have a close approximation to the true population statistics involving synthetic noise.

Using the above formulation the average cross power over the 10–12, 9–13 and 8–16 y bands is computed as a function of running time. These three bands, of progressively increasing width, are all centered around the well-known sunspot cycle

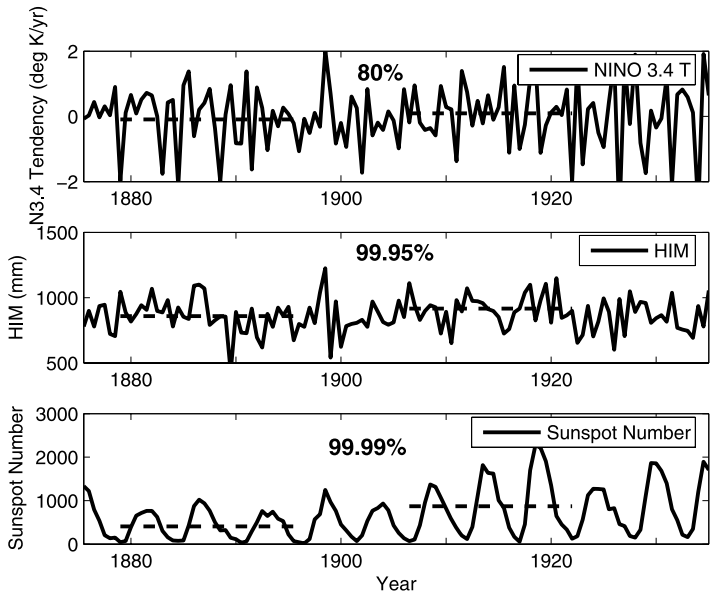

Fig. 1. The three time series analyzed. Also shown by bars across the time series are test periods 1 and 2, and the confidence level for rejection of the hypothesis that the averages over the two test periods are the same.

with a period of about 11.6 y, and serve to allow for the variations noticed in the sunspot period. The range of this variation is 9 to 13 y according to Lassen and Friis-Christensen [17], so the 9–13 y band is often preferred in the present analysis.

Over each of the two identified test periods of low and high solar activity, namely 1878–1913 and 1933–1964 respectively, the band-averaged cross powers between the sunspot index and the signals are compared with those of sunspot index and the matched noise samples. Confining attention to such test periods not only offers maximum possible contrast in solar activity signatures that may be present in the atmospheric indices, but also ensures that over the individual test periods the signals can be considered stationary to some good approximation. The comparison mentioned demands that we test whether differences between band-averaged coefficients of different kinds are significant. Several such differences between band-averaged signal and noise cross-spectra with sunspots, e.g. averaged values within either period or between test periods, are relevant for the present investigation.

We now introduce the following notation for the cross-spectral averages that form the chief objects of our analysis: (1) average over a band b, $R_b^{SS-SN}(t)$, function of running time, subscript b denoting band; (2) average over (noise) ensemble, $\langle R_b^{SS-SN}(t)\rangle$, function of running time and band; and (3) time-average over test period k, $[R_b^{SS-SN}(t)]_k$, function of band, $k = 1, 2$. For instance the cross-spectrum between sunspots and noise, in the 9–13 y band, averaged over the ensemble at each time, and then over time for test period 1, will be denoted by $[R_{9-13}^{SS-SN}(t)]_1$, which is just one number.

If $\overline{R}_1$ and $\overline{R}_2$ are the means of two band-averaged cross-spectra, we form the z-test statistic

$$z = \frac{(\overline{R}_1 - \overline{R}_2)}{\sqrt{[\mathrm{var}(\overline{R}_1)/n_1 + \mathrm{var}(\overline{R}_2)/n_2]}}, \tag{10}$$

where n_1, n_2 are the number of samples used to obtain the concerned averages. The z-test is adequate if the averages cover at least one test period, as we then have more than the 30 samples required for the test. We adopt the null hypothesis that there is no significant difference between the two means. The hypothesis is rejected at confidence level $100(1-\alpha)\%$ if $Z > z_\alpha$ for a one-sided test against the alternative hypothesis that the difference is greater than zero [5].

It is sometimes preferable to consider the cumulative distribution of cross-spectra and assess the difference between them by the χ^2 test. This has the advantage that the full distribution may provide additional insights beyond that from a test of the means.

6. Results

6.1. ENSO–solar activity–HIM rainfall

Fig. 1 shows the three major time series we analyze here: HIM rainfall (HR), the Nino 3.4 tendency (abbreviated N34T henceforth) and sunspot numbers (SS). Analysis of band-averaged cross-spectra (not presented here) shows that, among the total of seven Indian regional rainfall data sets considered by us, HIM rainfall has by far the highest values with N34T in

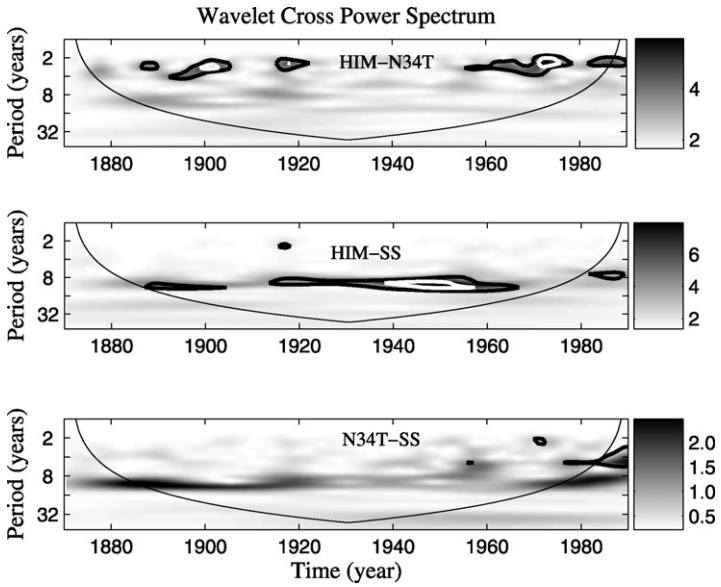

Fig. 2. Wavelet cross-spectra. Note that the HIM–N34T cross-spectrum reveals two significant bands, a strong one around 2–6 y and a modest one around 8–14 y.

the 8–16 y band (more than 2.5 times the next highest value). It is among the stronger ones in the 2–7 y band as well. We therefore select HIM rainfall and N34T for our illustrative analysis.

It is evident from Fig. 1 that both rainfall and the N34T index appear irregular and random, while sunspot numbers have a clear cyclic character. Comparisons over the two test-periods show that mean rainfall and solar activity increase and the N34T index decreases significantly from TP1 to TP2, the difference in means being significant by the z-test at confidence levels exceeding 80%, 99.99% and 99.95% for N34T, HIM rainfall and sunspot numbers respectively.

Fig. 2 shows maps of the wavelet cross-spectra between (a) HIM and N34T, (b) HIM and sunspot numbers, and (c) N34T and sunspot numbers. Outlined on these graphs are contours enclosing regions where wavelet cross power is significantly higher, at 90% and 95% confidence levels with respect to the reference spectra of Eq. (10). It is noticed that the HIM–N34T cross-spectra show the highest values in the 2–5 y band, but intermittently. There is high cross power in the 2–6 y period band particularly over 1990–2000; but it is low in the 8–16 y period band compared to that over the first test period. This may be attributed to higher N34T over the period 1990–2000 as compared to sunspot numbers, which were not so high over the same period. There is also appreciable strength in the solar cycle band around 8–12 y. In the cross-spectra with sunspots the highest power is in the 8–16 year period band in both cases, and the powers are higher during the test periods. In the case of the cross-spectrum between N34T and sunspot numbers, the higher power occurs over the period 1880–1910 in the 8–16 y band.

Fig. 3 summarizes the distribution of band-averaged cross power across the bands for the three variable-pairs we are analyzing. Band-widths vary by octaves beginning with 1–2 y period. (Band-widths quoted are closed at the left end and open at the right, in analogy with open and closed intervals in mathematical analysis; e.g. the 4–8 y band covers the periods 4, 5, 6, 7 y.) It is seen that the HIM–N34T cross-spectrum peaks in band 2 (2–4 y), and is appreciable in bands 3 (4–8 y) and 4 (8–16 y) as well. HIM–sunspot has a strong peak (53% of total) in band 4, the next highest being only 17%. The N34T–sunspot distribution also peaks in band 4 (about 48%), the next highest being about 20% in band 3. The interesting conclusion from Fig. 3 is that rainfall–sunspot connections are strong, ENSO–sunspot only slightly less so; the rainfall–ENSO connections are spread over three bands, the strongest being 2–4 y but the next highest being 4–8 and 8–16 y, covering the solar cycle and its harmonics.

As the cross power resides largely in two bands, Fig. 4 shows averages over the 2–7 y and 9–13 y bands, for the same three variable-pairs discussed above. This diagram is more revealing than either Fig. 1 or Fig. 2 in terms of the effect of solar activity. Considering first the connections between HIM and N34T, it is seen that the cross power is much higher in the 2–7 y band than in the 9–13 y band (note the different ordinate scales in the top and bottom panels of Fig. 4). Thus, in TP1 the cross power in the 2–7 y band is about nine times higher than in the 9–13 y band. In TP2 the factor is about twice as large. However, if we look at the HIM/sunspot cross-spectra, it is clearly higher in the 9–13 y band than in the 2–7 y band.

Coming to N34T and sunspots we see that the cross-spectrum in the 9–13 y band is higher (/lower) than that in the 2–7 y band in TP1 (/TP2). Thus, while the rainfall cross power increases with solar activity in both bands, we have the intriguing conclusion that the N34T cross power increases with solar activity in the 2–7 y band and decreases in the 9–13 y band. The contrast between the two bands we are considering is clearly visible from the bottom panel of Fig. 4.

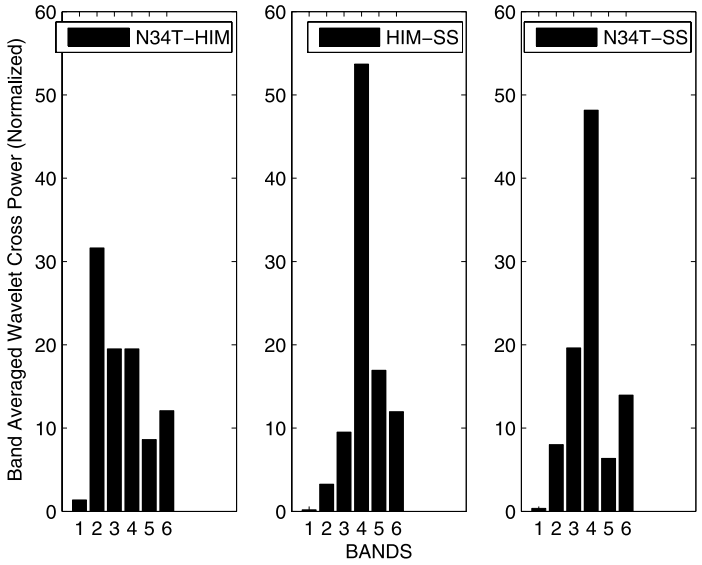

Fig. 3. Band-averaged wavelet cross power as percentage of total, for the pairs HIM–N34T, HIM–SS, N34T–SS. The period range in the different bands are as follows: Band (1) 1–2 y, (2) 2–4 y, (3) 4–8 y, (4) 8–16 y, (5) 16–32 y, (6) 32–64 y.

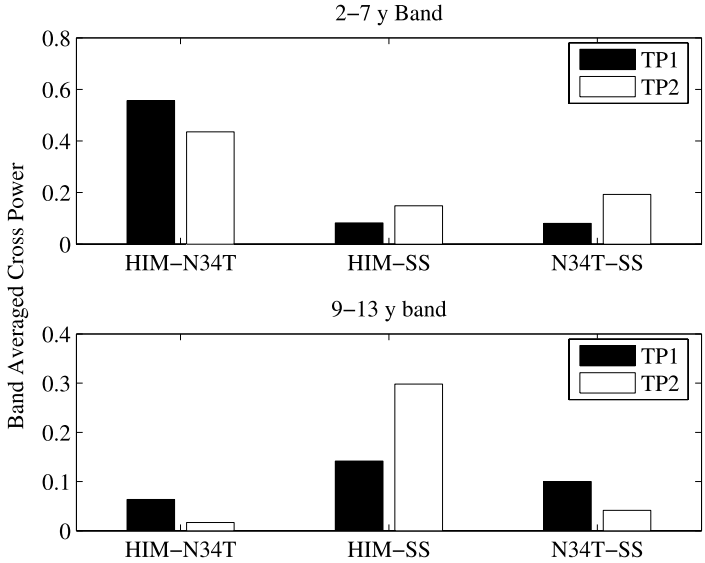

Fig. 4. Band-averaged cross power between pairs of the three time series of Fig. 1 in each of the two test periods.

Fig. 5 presents data on the cumulative distribution function (CDF) of the cross power between the three variable-pairs in the 2–7 y and 9–13 y bands and the two test periods. The CDF of the HIM–N34T cross-spectrum is quite different from the other two, which incidentally almost coincide. This is consistent with the data in Fig. 4, and suggests that the connection between sunspots and either rainfall or N34T is weaker than that between N34T and rainfall when solar activity is low. In the 9–13 y band however there is a distinct difference, and the connection gets less strong as we go from rainfall/sunspots to N34T/sunspots to N34T/rainfall. In TP2 the relations in the 2–7 y band are not dramatically different from those in TP1, but in the 9–13 y band the HIM–sunspot relation is much higher than are the other two, the cross-spectrum between sunspots and N34T being once again higher than that between rainfall and N34T.

Figs. 6 and 7 present comparisons of observed cross-spectra of N34T against those with spectrally matched noise, respectively for the 2–7 and 9–13 y bands. In either case it will be noticed that the N34T–SN data are not very different between the two test periods (note that the abscissa scales vary within and between the two diagrams). However, in the 2–7 y band the CDF of the N34T–SS cross-spectrum moves substantially to the right in TP2 – from a median of nearly 0.08 to more than 0.16, the highest value of R_{2-7} increasing from about 0.125 in TP1 to slightly more than 0.4 in TP2.

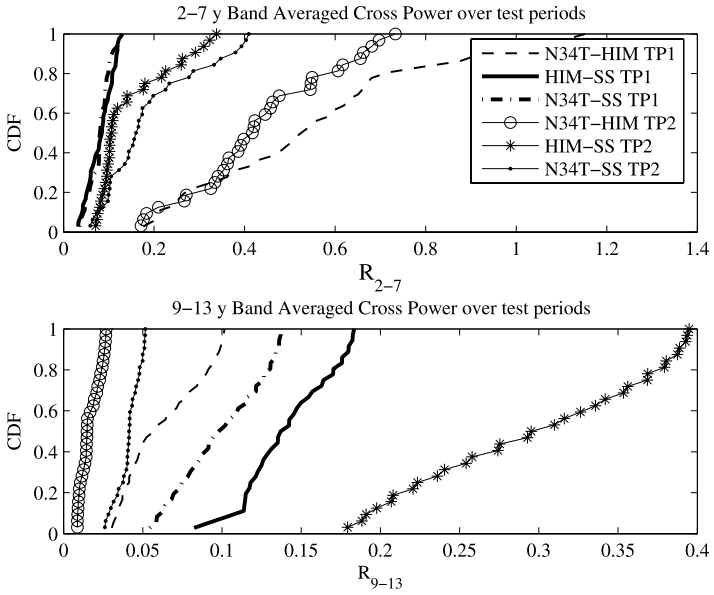

Fig. 5. Cumulative distribution function of 2–7 y and 9–13 y band-averaged cross-spectra between paired variables over test periods 1, 2.

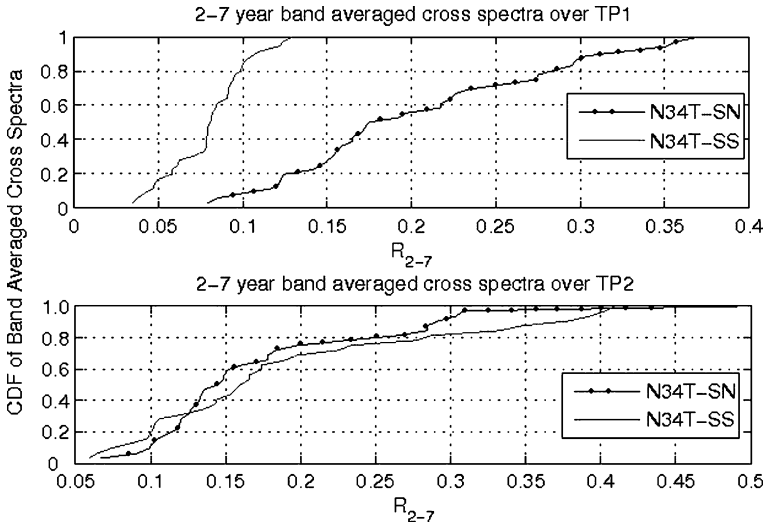

Fig. 6. Cumulative distribution function 2–7 y band-averaged cross-spectra between N34T sunspot numbers and N34T as well as spectrally matched noise, over each test period.

In the 9–13 y band too (Fig. 7) the N34T–SN curve does not change much between the test periods, but N34T–SS curve moves substantially again, but this time to lower values – i.e. in the direction opposite to that seen in Fig. 6. Thus the median drops from about 0.1 to 0.041, and the highest value of R_{9-13} from nearly 0.14 to about 0.051 – a factor in the range between 2.5 to 3.

In both bands, the change in the cross-spectra of sunspots and N34T is very significantly different from that in the case of sunspots and spectrally matched noise.

These figures indicate that the characteristics of the CDF of the cross-spectra with sunspots can be very different from those with noise. Interestingly the differences are larger when the solar activity is lower; and the range of values of the cross-spectra with sunspots is lower and more concentrated than with noise. For both 2–7 y and 9–13 y bands, the hypothesis that N34T–SS cross-spectra CDF come from the same population distribution as the N34T–SN pair is rejected at greater than 99.5% confidence by the χ^2 test (four degrees of freedom).

We make one final comment in passing. If we make the same analysis for the global ENSO index (EN) and AISMR, we find that higher solar activity *increases* the wavelet power in EN and reduces that in AISMR in the 2–7 y band. (The effects of solar activity on EN and N34T are therefore opposite in sign to each other.) In the 8–16 y band the effects are the

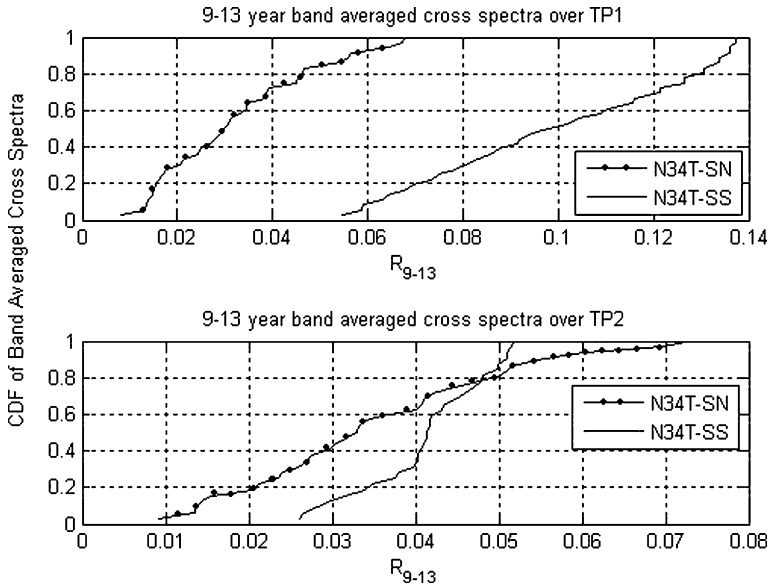

Fig. 7. Same as Fig. 5, but for the 9–13 y band.

same as on N34T and HR. This finding highlights the point made in Section 2, about the need for taking meteorological heterogeneity into account. This issue will be addressed separately.

7. Discussion

In the work reported here, the connections between solar activity and rainfall or ENSO time series are found to be statistically highly significant, especially when they are studied over contrasting epochs of respectively high and low solar activity. In contrast, the correlation between a full time series of an atmospheric process with the solar cycle (over a duration of 120 y say) often yields negligible correlation coefficients [12,16]. ENSO covaries with high solar activity epochs negatively, at significance levels exceeding 97%. Sunspots and rainfall averaged over periods of order 30 y covary at higher significance levels than do ENSO and rainfall (80%). (However contributions to rainfall power from ENSO are a factor of 3–4 higher.)

The results from the wavelet cross-spectral analysis provide confirmatory but far more detailed evidence for the above conclusions. Our results broadly agree with those outlined by [19] regarding the influence of ENSO and sunspot numbers on AISMR. However, the connections between ENSO and solar activity come out to be stronger than those between rainfall and ENSO, and in particular differ regarding the role of the 11 y cycle. The statistical significance tests performed here on both the raw time series and the wavelet cross-spectra, with sample sizes respectively greater than 30 and 119, do not suffer from dearth of number of sample points as in the methods used by Mehta and Lau. Their method involved an analysis of rainfall, SST and irradiance using a narrow band Fourier filter centered at the 11 year period and hence isolates a cycle with a specific period. They concluded that there was no consistent relationship between the 11 year components of solar irradiance and either the monsoon rainfall or the Nino 3 SST. Contrary to this conclusion, the present study finds that not only the rainfall but also ENSO show significant cross-spectra with sunspots and other related parameters in the middle of the 8–16 y period band. We consider that in a nonlinear process that involves interactions over several time (and space) scales, appropriate band averages can provide more insight. The ENSO index by itself has a rather flat but high power spectrum in the 2–7 year band, and shows comparable power in the 8–32 y band. The rainfall shows various periods, and the well-known solar cycle around 11.6 y has a cycle length varying between 9 and 13 y as already mentioned, and contains both harmonics and subharmonics.

As regards the connections of rainfall with N34T our results agree with those reported by Rajeevan et al. [27] regarding the robust inverse relationship. Our results also confirm that over the 1970–2000 period, the so-called ENSO–monsoon inverse relationship has weakened, as already reported by Krishna Kumar [15]. There clearly are epochs over which the ENSO–monsoon relationship experiences a decreasing correlation, as suggested by Maraun and Kurths [19].

Band-averaged cross power between N34T and rainfall is higher in the first test period than in the second, but that between sunspots and rainfall shows a trend opposite to that of ENSO–rainfall over both bands under consideration. Finally the ENSO–sunspot band-averaged cross power in TP2 is higher than in TP1 in the 2–7 year band, but lower in the 8–16 y band.

8. Conclusions

Our conclusions may be summarized as follows.

First of all the mean Pacific SST anomalies related to ENSO are higher (/lower) in the lower (/higher) solar activity period. The wavelet spectra of HIM rainfall show substantial power in the 8–16 y period band (25.2%). Contribution to N34T from the same band is 12.9%. These conclusions are consistent with the well-known inverse relationship between ENSO and rainfall, leading to higher (/lower) rainfall in periods of lower (/higher) ENSO indices and higher (/lower) solar activity. Even in these cases, the confidence levels at which the differences (in band-averaged wavelet power over two test-periods of maximum contrast in solar activity) are significant are about 97.5% for the 10–12 y and 9–13 y bands in the case of Nino 3.4T.

Interestingly, there is considerable power (approximately 13.5% and 56.8% respectively) in the wavelet cross power spectra in both 2–7 y and 8–16 y period bands for the HIM/sunspot pair. The 2–7 y period band contains most of the cross power (34.3%) in the case of N34T/HIM rainfall, while the 8–16 y period band contains most of the cross power (56.8%) in the case of solar/rainfall indices.

The detailed study of the variability of the ENSO–monsoon–sunspot triad over the two epochs of high and low solar activity (TP1 and TP2) suggests a somewhat complex relationship on the 2–7 y time scale; an increase in solar activity reduces both the N34T index and rainfall marginally. But the situation is different in the 8–16 y band, where an increase in solar activity is associated with a drastic reduction in N34T and an appreciable increase in the rainfall. The net effect of solar activity on rainfall therefore appears to be the result of cooperating or counteracting influences on the short and long periods, depending on the indices used; scale-interactions therefore appear to be important.

Nevertheless, the link between monsoon rainfall and solar activity emerges as having the strongest evidence; next comes the ENSO–solar activity connection, which is stronger than the ENSO–monsoon connection.

As we have already pointed out in Section 2, the present analysis is concerned only with scales longer than 2 years; further solar cycles have lengths varying from 9–13 years and the present statistical analysis deals with averages over test periods of three solar cycles. Considering these facts, our major conclusions here are concerned with what Kodera [14] has termed 'multi-decadal' connections. We may therefore state our conclusions as follows.

The evidence for such 'multi-decadal' connections between Indian rainfall and solar activity, directly and mediated through ENSO, is strong, as tested by two different procedures: time-domain analysis (which uses sunspot numbers only to select periods of greatest contrast in solar activity) and wavelet cross-spectra (band-averaged and otherwise, which use quantitative solar activity data to analyze effects in different period bands).

The differences in cross-spectra of rainfall and ENSO variables with sunspots and with the respective spectrally matched noise are significant. As spectra convey only information on energy content in different frequency bands, and in particular lose information on phase relations between different frequencies, the differences with spectrally matched noise must be attributed to the special phase relations between solar activity and rainfall/ENSO. The Monte Carlo procedures devised here help to reveal such subtle phase relationships. A more detailed analysis of such relationships will be presented separately.

Acknowledgments

R.N. acknowledges financial support from project DRDO/RN/4124, and the continued hospitality of the Centre for Atmospheric and Oceanic Sciences at the Indian Institute of Science, Bangalore. He is also grateful to Prof. Marie Farge and CIRM in France and NBHM in India for enabling his visit to Marseilles for attending the Symposium in honor of Jean Morlet.

References

[1] S. Baliunas, P. Frick, D. Sokoloff, W. Soon, Time scales and trends in the central England temperature data (1659–1990): A wavelet analysis, Geophys. Res. Lett. 24 (1997) 1351–1354.
[2] J. Beer, et al., Use of ^{10}Be in polar ice to trace the 11-year cycle of solar activity, Nature 347 (1990) 164–166.
[3] S. Bhattacharyya, R. Narasimha, Possible association between Indian monsoon rainfall and solar activity, Geophys. Res. Lett. 32 (2005), doi:10.1029/2004GL021044.
[4] S. Bhattacharyya, R. Narasimha, Regional differentiation in multidecadal connections between Indian monsoon rainfall and solar activity, J. Geophys. Res. 112 (2007), doi:10.1029/2006JD008353, D24103.
[5] E.L. Crow, F.K. Davis, M.W. Maxfield, Statistics Manual: With Examples Taken from Ordnance Development, Dover, Mineola, NY, 1960.
[6] N. Delprat, B. Escudie, P. Guillemain, R. Kronland-Martinet, P. Tchamitchian, B. Torresani, Asymptotic wavelet and Gabor analysis: Extraction of instantaneous frequencies, IEEE Trans. Inform. Theory 38 (2) (1992) 644–664.
[7] M. Fligge, S.K. Solanki, J. Beer, Determination of solar cycle length variations using the continuous wavelet transform, Astron. Astrophys. 346 (1999) 313–321.
[8] P. Frick, D. Galyagin, D. Hoyt, E. Nesme-Ribes, K. Shatten, D. Sokoloff, V. Zakharov, Wavelet analysis of solar activity recorded by sunspot groups, Astron. Astrophys. 328 (1997) 670–681.
[9] E. Friis-Christensen, K. Lassen, Length of the solar cycle: An indicator of solar activity closely associated with climate, Science 254 (1991) 698–700.
[10] M. Grigoriu, On the spectral representation method in simulation, Probab. Eng. Mech. 8 (1984) 610–620.
[11] J.D. Haigh, M. Blackburn, R. Day, The response tropospheric circulation to perturbations in lower stratospheric temperature, J. Clim. 18 (2005) 3672–3691.
[12] P. Jagannathan, H.N. Bhalme, Changes in the pattern of distribution of southwest monsoon rainfall over India associated with sunspots, Monthly Weather Rev. 101 (9) (1973) 691–700.
[13] S.V. Kailas, R. Narasimha, Quasi cycles in monsoon rainfall using wavelet analysis, Current Sci. 78 (2000) 592–595.
[14] K. Kodera, Possible solar modulation of the ENSO cycle, Pap. Met. Geophys. 55 (2005) 21–32.
[15] K. Krishna Kumar, On the weakening relationship between the Indian monsoon and ENSO, Science 284 (1999) 2156.
[16] K. Labitzke, H. van Loon, The signal of the 11-year sunspot cycle in the upper troposphere–lower stratosphere, Space Sci. Rev. 80 (1997) 393–410.

[17] K. Lassen, E. Friis-Christensen, Variability of the solar cycle length during the past five centuries and the apparent association with terrestrial climate, J. Atmos. Terr. Phys. 57 (8) (1995) 835–845.
[18] B. Liu, D.C. Mundson, Generation of a random sequence having a jointly specified marginal distribution and autocovariance, IEEE Trans. Acoust. Speech Signal Process. 30 (6) (1982) 973–983.
[19] D. Maraun, J. Kurths, Cross wavelet analysis: Significance testing and pitfalls, Nonlinear Process. Geophys. 11 (2004) 505–514.
[20] V. Mehta, K.M. Lau, Influence of solar irradiance on the Indian monsoon–ENSO: Relation at decadal–multidecadal time scales, Geophys. Res. Lett. 24 (1997) 159–162.
[21] G.A. Meehl, J.M. Arblaster, K. Matthes, F. Sassi, H. van Loon, Amplifying the pacific climate system response to a small 11-year solar cycle forcing, Science 325 (2009) 1114–1118.
[22] R. Narasimha, S.V. Kailas, A wavelet map of monsoon variability, Proc. Indian Nat. Sci. Acad. 67 (2001) 327–341.
[23] U. Neff, S.J. Burns, A. Mangini, M. Mudelsee, D. Fleitmann, A. Matter, Strong coherence between solar variability and the monsoon in Oman between 9 and 6 kyr ago, Nature 411 (2001) 290–293.
[24] E. Nesme-Ribes, P. Frick, D. Sokoloff, V. Zakharov, J.-C. Ribes, A. Vigouroux, F. Laclare, Wavelet analysis of Maunder minimum as recorded in Solar diameter data, C. R. Acad. Sci. Paris Ser. IIB 321 (1995) 525–532.
[25] B. Parthasarathy, A.A. Munot, D.R. Kothawale, Homogeneous Indian monsoon rainfall: Variability and prediction, Proc. Indian Acad. Sci. (Earth and Planetary Science) 102 (1993) 121–155.
[26] B. Parthasarathy, A.A. Munot, D.R. Kothawale, Monthly and seasonal rainfall series for all-India homogeneous regions and meteorological subdivisions: 1871–1994, Research Report No. RR-065, Ind. Inst. Trop. Met., Pune, 1995.
[27] M. Rajeevan, D.S. Pai, R. Anil Kumar, New statistical models for long range forecasting of south-west monsoon rainfall over India, NCC Research Report 1, Ind. Met. Dept., Pune, 2005.
[28] A. Rai Choudhuri, The solar dynamo, Current Sci. 77 (11) (1999) 1475–1486.
[29] G. Saracco, N. Thouveny, D.L. Bourles, J.T. Carcaillet, Extraction of non-continuous orbital frequencies from noisy insolation data and from paleoproxy records of geomagnetic intensity using the phase of the continuous wavelet transforms, Geophys. J. Int. 176 (3) (2009) 767–781.
[30] C. Torrence, G.P. Compo, A practical guide to wavelet analysis, Bull. Amer. Met. Soc. 79 (1) (1998) 61–78.
[31] C. Torrence, P.J. Webster, The annual cycle of persistence in the El Nino/Southern Oscillation, Quart. J. Roy. Met. Soc. 124 (1998) 1985–2004.
[32] C. Torrence, P.J. Webster, Interdecadal changes in the ENSO–monsoon system, J. Clim. 12 (1999) 2679–2690.
[33] K.E. Trenberth, The definition of El Niño, Bull. Amer. Met. Soc. 78 (1997) 2771–2777.
[34] H. van Loon, G.A. Meehl, J.M. Arblaster, A decadal solar effect in the tropics in July–August, J. Atmos. Sol. Terr. Phys. 66 (2004) 1767–1778.